



## Experimental and Computational Studies on the 1:1 Complex of Anthranilic Acid with *P*-Toluenesulfonic Acid

İbrahim Şen , Cem Burak Yildiz , Hulya Kara & Akin Azizoglu


To cite this article: İbrahim Şen , Cem Burak Yildiz , Hulya Kara & Akin Azizoglu (2013) Experimental and Computational Studies on the 1:1 Complex of Anthranilic Acid with *P*-Toluenesulfonic Acid, Phosphorus, Sulfur, and Silicon and the Related Elements, 188:11, 1621-1633, DOI: [10.1080/10426507.2013.777724](https://doi.org/10.1080/10426507.2013.777724)


To link to this article: <https://doi.org/10.1080/10426507.2013.777724>

 View supplementary material [↗](#)

 Accepted author version posted online: 05 Apr 2013.  
Published online: 20 Sep 2013.

 Submit your article to this journal [↗](#)

 Article views: 150

 View related articles [↗](#)

 Citing articles: 2 View citing articles [↗](#)

## EXPERIMENTAL AND COMPUTATIONAL STUDIES ON THE 1:1 COMPLEX OF ANTHRANILIC ACID WITH P-TOLUENESULFONIC ACID

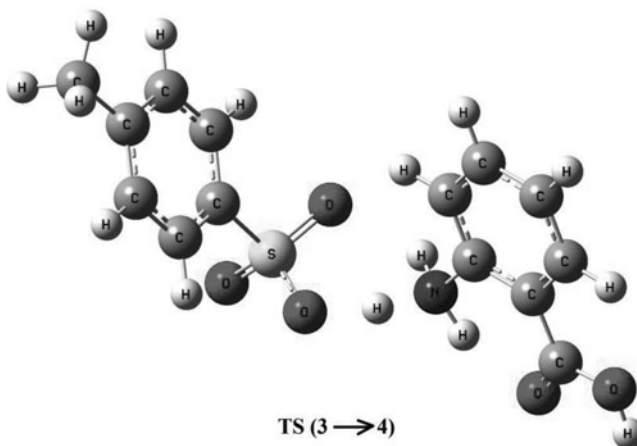
Ibrahim Şen,<sup>1</sup> Cem Burak Yildiz,<sup>1,2</sup> Hulya Kara,<sup>3</sup>  
and Akın Azizoglu<sup>1</sup>

<sup>1</sup>Department of Chemistry, Faculty of Arts and Sciences, University of Balıkesir,  
Balıkesir, Turkey

<sup>2</sup>Department of Chemistry, Faculty of Arts and Sciences, University of Aksaray,  
Aksaray, Turkey

<sup>3</sup>Department of Physics, Faculty of Arts and Sciences, University of Balıkesir,  
Balıkesir, Turkey

### GRAPHICAL ABSTRACT



**Abstract** The proton-transfer compound (**3**) was synthesized in good yields by the reaction of anthranilic acid with *p*-toluenesulfonic acid. It was characterized by elemental analysis, infrared spectroscopy, and X-ray single-crystal determination. The crystal structure analysis of 2-carboxyanilinium *p*-toluenesulfonate (**3**) has revealed a one-dimensional hydrogen-bonded

Received 22 November 2012; accepted 15 February 2013.

The authors are indebted to the Scientific and Technical Research Council of Turkey (TUBITAK) and University of Balıkesir for their financial support. Dr. Kara would like to thank TUBITAK for NATO-B1 and the Royal Society short visit fellowship for financial support and Prof. Guy Orpen (School of Chemistry, University of Bristol, UK) for his hospitality. The authors are also very grateful to Dr. Mairi F. Haddow (The School of Chemistry, University of Bristol) for the X-ray measurements.

Address correspondence to Akın Azizoglu, Department of Chemistry, Faculty of Arts and Sciences, University of Balıkesir, TR-10145 Balıkesir, Turkey. E-mail: azizoglu@balikesir.edu.tr

network structure, involving the tosylate anion, the carboxyl group, and the ammonium group. The  $H(N)\cdots O$  distances range from 1.97 to 2.23 Å. The molecular geometry and vibrational frequencies of **3** were calculated using the *ab-initio* method (HF) with the 6-31G(d) and 6-31+G(d,p) basis sets. The computed results indicate that the optimized geometry reproduces the crystal structure well, and the assignments of fundamental vibrations also agree well with the theoretical frequencies. The intermolecular proton transfer process between the ionic (**3**) and nonionic (**4**) structures was also investigated with the theoretical computations. The nonionic form (**4**) is energetically more stable than the ionic form (**3**) and **TS(3→4)** by 9.76 and 7.01 kcal/mol, respectively, including the zero-point vibrational energy correction at the HF/6-31+G(d,p) level. In addition, the atomic charges, the molecular electrostatic potentials, the nucleus-independent chemical shifts, and the frontier molecular orbitals of **3** were carried out at the HF/6-31+G(d,p) level of theory.

Supplementary materials are available for this article. Go to the publisher's online edition of Phosphorus, Sulfur, and Silicon and the Related Elements for the following free supplemental files: Additional figures and tables

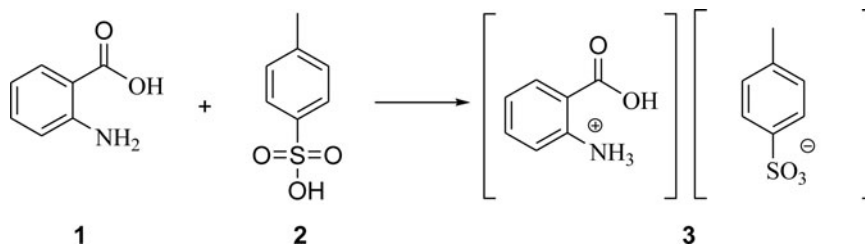
**Keywords** Proton transfer compound; FTIR spectra; crystal structure; Hartree–Fock method; NICS analysis

## INTRODUCTION

The chemistry of anthranilic acid (2-aminobenzoic acid, **1**) is of importance in medicinal and biological chemistry because it is the biochemical precursor to the amino acid tryptophan, as well as a catabolic product of tryptophan in animals.<sup>1–3</sup> It is also integrated into many alkaloids isolated from plants. Like other amino acids, anthranilic acid is amphoteric. Due to the electron donating effect of the amino group, anthranilic acid is a weaker acid than benzoic acid. It also contains both a hydrogen bond acceptor and a donor that are conjugated. As a base, anthranilic acid is much weaker than aniline because of the pronounced electron-withdrawing effect of the carboxyl function.<sup>1</sup>

In the past few decades, there has been an enormous amount of interest in proton transfer self-associated systems because intra- or intermolecular proton transfer exhibits potential for the control of a variety of physical properties of organic solids.<sup>4–12</sup> The intermolecular bond in such systems may consist of ion-pairing, hydrogen bonding, hydrophobic or hydrophilic, host–guest,  $\pi$ – $\pi$  stacking, and donor–acceptor interactions. In an ideal case, one or combination of some of these intermolecular bonding processes may result in the formation of specific and spontaneous self-associated forms of the desired aggregate. Although there have been several experimental and theoretical studies on proton transfer between a carboxylic acid and an amine,<sup>9–12</sup> the crystal structures of proton transfer compounds with toluene-4-sulfonic acid (or *p*-toluenesulfonic acid, PTSA, **2**) are uncommon, possibly because of the absence of interactive functional substituent groups to promote secondary hydrogen bonding extension.<sup>13,14</sup>

Herein, we have prepared a novel proton transfer compound obtained from anthranilic acid and PTSA (Scheme 1). The optimal geometry and the detailed vibrational analysis of the title ion pair (**3**) with the help of theoretical and spectroscopic methods have been also reported in detail. Moreover, the molecular electrostatic potential maps, natural bond orbitals, frontier molecular orbitals, and nucleus-independent chemical shifts (NICS) have been calculated at the HF/6-31G(d) and the HF/6-31+G(d,p) levels. These studies are valuable for providing insight into molecular properties of proton transfer compounds.



**Scheme 1** Synthetic route to prepare the 2-carboxyanilinium *p*-toulenesulfonate (3)

## RESULTS AND DISCUSSION

### Description of the Crystal Structure

Table 1 lists the experimental parameters used for data collection and determination of the structure (3). The crystal structure of the 1:1 proton transfer compound of anthranilic acid with PTSA ( $\text{C}_7\text{H}_8\text{NO}_2^+ \cdot \text{C}_7\text{H}_7\text{O}_3\text{S}^-$ ), 3, is also depicted in detail (Figure 1). Hydrogen bond motifs are commonly used as a way of guiding the interactions between molecules. It is important to understand what a likely outcome is for functional group interactions between molecules. As can be seen from Figure 2, the N–H...O(C) and N–H...O(S) intramolecular hydrogen bonds and the N–H...O(S) and O–H...O(S) type intermolecular hydrogen bonds are formed in 3. Three hydrogen donors of the protonated amine group give direct hydrogen bonding associations, with three of the sulfonate O-atom acceptors from three independent

**Table 1** Crystal data and structure refinement for 3

|  |  |                            |
|--|--|----------------------------|
| Empirical formula  | $\text{C}_{14}\text{H}_{15}\text{NO}_5\text{S}$  |                            |
| Formula weight ( $\text{g mol}^{-1}$ )                         | 309.33   |                            |
| Temperature (K)  | 100(2)   |                            |
| Crystal system   | Triclinic  |                            |
| Space group  | P-1  |                            |
| Unit cell dimensions   | $a = 6.3703(5) \text{ \AA}$                      | $\alpha = 93.156(2)^\circ$ |
|  | $b = 9.0379(6) \text{ \AA}$                      | $\beta = 90.301(3)^\circ$  |
|  | $c = 11.8521(8) \text{ \AA}$                     | $\gamma = 92.883(3)^\circ$ |
| Volume ( $\text{\AA}^3$ )                                      | 680.46(8)  |                            |
| Z  | 2  |                            |
| Density (calculated) ( $\text{g/cm}^{-3}$ )                    | 1.510  |                            |
| Absorption coefficient ( $\text{mm}^{-1}$ )                    | 0.260  |                            |
| $\theta$ range for data collection                             | 1.72 to 27.60°                                   |                            |
| <i>hkl</i> ranges  | $-7 < h < 8$<br>$-11 < k < 11$<br>$-14 < l < 15$ |                            |
| Reflections collected  | 7208   |                            |
| Independent reflections  | 3142 [ <i>R</i> <sub>int</sub> = 0.0278]         |                            |
| Refinement method  | Full-matrix least squares on $F^2$               |                            |
| Data/restraints/parameters                                     | 3142/0/193                                       |                            |
| Goodness-of-fit on $F^2$                                       | $S = 1.054$                                      |                            |
| <i>R</i> indices [for 2741 reflections with $I > 2\sigma(I)$ ] | $R^1 = 0.0353$ , $wR^2 = 0.0923$                 |                            |
| <i>R</i> indices (for all 3142 data)                           | $R^1 = 0.0415$ , $wR^2 = 0.0969$                 |                            |
| Largest diff. peak and hole                                    | 0.402 and $-0.479 \text{ e\AA}^{-3}$             |                            |

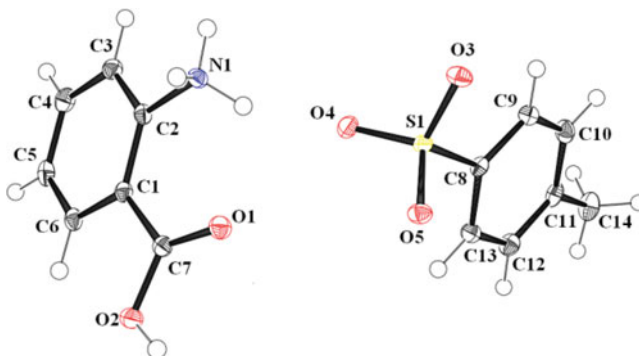


**Figure 1** The ORTEP illustration of **3**. (Displacement capped sticks are plotted at the 50% probability level) (Color figure available online).

PTSA anions [N...O distances: N1...O5<sup>i</sup> = 2.8475(17), N1...O3<sup>ii</sup> = 2.7725(17) and N1...O4 = 2.9751(17) Å; symmetry codes: (i)  $[-x, -y, 1 - z]$ , (ii)  $[1 - x, -y, 1 - z]$ . Moreover, the O2...O4<sup>iii</sup> = 2.6392(16) [iii =  $-1 + x, y, z]$  and N1...O1 = 2.6565(17) hydrogen bonds are formed in **3**. These result in a linear polymer structure extending along the *a* axis.

The hydrogen-bonded geometry and details are listed in Table 2. For the complex (**3**), where the interacting units appear, the N—H...O hydrogen bonds are formed between PTSA and anthranilic acid. Analysis of hydrogen bonds in **3** reveals that all potential donor/acceptor groups are involved in intermolecular interactions. The delocalization in complex (**3**) involves the weak interaction of the N(1)—H(1C) bonding with the S(1)—O(4) antibonding. This interaction affects the stabilization of complex (**3**), by very low energy, 0.17 kcal/mol, computed by the NBO analysis.

### Optimized Geometries

The ionic (**3**) and nonionic (**4**) structures were optimized at the HF/6–31G(d) and the HF/6–31+G(d,p) levels. The calculated geometrical parameters of **3** and **4** are summarized in Table 3 in accordance with its atom numbering scheme, shown in Figure 2. It can be indicated for the structural data of **3** that there is a rather good agreement between our

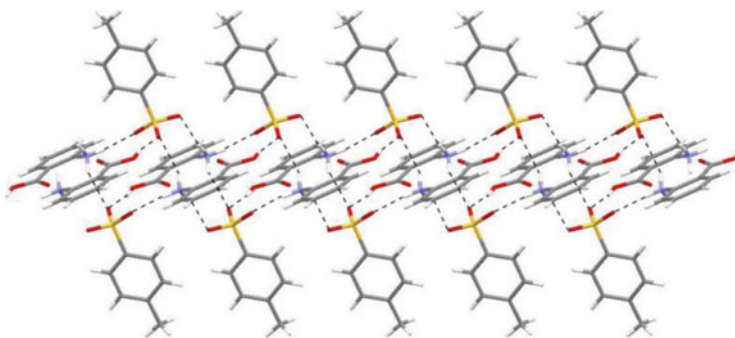


**Figure 2** MERCURY view of the one-dimensional structure of **3** along *a*-axis. H-bonding interactions are represented by dotted lines (Color figure available online).

**Table 2** Geometry of hydrogen bonds (Å) for **3**

| D—H...A                   | D—H (Å) | H...A (Å) | D...A (Å)  | DHA (°) |
|---------------------------|---------|-----------|------------|---------|
| N1—H1A...O5 <sup>i</sup>  | 0.91    | 1.97      | 2.8475(17) | 161.00  |
| N1—H1B...O3 <sup>ii</sup> | 0.91    | 1.87      | 2.7725(17) | 173.00  |
| N1—H1C...O1               | 0.91    | 2.23      | 2.6565(17) | 108.00  |
| N1—H1C...O4               | 0.91    | 2.18      | 2.9751(17) | 146.00  |
| O2—H2...O4 <sup>iii</sup> | 0.84    | 1.81      | 2.6392     | 168.00  |

<sup>i</sup>Symmetry codes:  $[-x, -y, 1 - z]$ <sup>ii</sup>Symmetry codes:  $[1 - x, -y, 1 - z]$ <sup>iii</sup>Symmetry codes:  $[-1 + x, y, z]$ 

theoretical calculations and the experimental ones (Table 3). Especially, the calculated value of O(4)—H(1C) (1.830 Å) distance is found to be much shorter than the X-ray data of 2.176 Å for **3**, whereas that of N(1)—H(1C) (1.032 Å) bond length is a little longer than the experimental one 0.910 Å at the level of HF/6-31+G(d,p) theory. The discrepancy between the experimental (X-ray) and calculated values for the atomic coordinates might result from the different environments of a molecule in the experimental crystalline state and in the theoretical gas phase. However, it may be stated that the modeling techniques applied in the present work properly reflect the main properties of the actual structure and can be successfully applied for predicting the features of the title molecule **3**.

The transition structures (**TS3**→**4**) for the proton transfer between the ionic (**3**) and nonionic (**4**) structures were determined successfully, and their relative energies were also calculated at the HF/6-31+G(d,p) level (Figure 3). In other words, the intermolecular proton transfer process **3**→**TS**→**4** was investigated with the theoretical computations at the gas phase. Because of the migration of a hydrogen atom from atom N1 to atom O4, some changes are observed between **3** and **4**. The distance between atoms O4 and H(1C) decreases upon the proton transfer **3**→**TS**→**4**. The N1—H(1C) and O4—H(1C) distances are found to be 1.032 Å and 1.830 Å for **3**, 1.190 Å and 1.282 Å for **TS**, and 1.919 Å and 0.968 Å for **4**, respectively (Table 3). Besides, the nonionic form (**4**) is energetically more stable than the ionic form (**3**) by 9.76 kcal/mol, including the zero-point vibrational energy correction at the HF/6-31+G(d,p) level. The activation energy barrier for the proton transfer of PTSA to anthranilic acid is also found to be quite low, by 7.01 kcal/mol (Figure 3). From X-ray measurements, the complex (**3**) is found to be in the ionic form, whereas in the gas phase the charge separation is destabilized by the absence of intermolecular bonding interactions from the surrounding media.

### Vibrational Spectra

The FT-IR spectrum of the title ion-pair (**3**) was recorded in the 4000–400 cm<sup>-1</sup> region using KBr pellets on a Perkin-Elmer 1600 series FTIR spectrophotometer. Harmonic vibrational frequencies of **3** were also computed at the HF/6-31G(d) and the HF/6-31+G(d,p) levels. The vibrational band assignments were carried out using the GaussView molecular visualization program. In order to facilitate assignment of the observed peaks, we have analyzed the vibrational frequencies and compared our theoretical calculation for **3** with the experimental results (see supplemental data Table S1, available online). The assignment of the experimental frequencies is based on the observed band frequencies in the infrared

**Table 3** Selected experimental and theoretical bond lengths (Å) and angles (°) of **3**, **4**, and related transition structure (**TS**)

|                     | 3               |             |                | TS          |                |             | 4              |             |                |
|---------------------|-----------------|-------------|----------------|-------------|----------------|-------------|----------------|-------------|----------------|
|                     | X-ray data of 3 | HF/6-31G(d) | HF/6-31+G(d,p) | HF/6-31G(d) | HF/6-31+G(d,p) | HF/6-31G(d) | HF/6-31+G(d,p) | HF/6-31G(d) | HF/6-31+G(d,p) |
| S(1)–O(3)           | 1.456           | 1.473       | 1.472          | 1.432       | 1.433          | 1.424       | 1.422          | 1.422       | 1.422          |
| S(1)–C(8)           | 1.773           | 1.775       | 1.776          | 1.767       | 1.769          | 1.758       | 1.760          | 1.758       | 1.760          |
| O(1)–C(7)           | 1.215           | 1.197       | 1.199          | 1.197       | 1.198          | 1.197       | 1.199          | 1.197       | 1.199          |
| O(2)–C(7)           | 1.323           | 1.318       | 1.317          | 1.321       | 1.320          | 1.328       | 1.327          | 1.328       | 1.327          |
| O(2)–H(2)           | 0.840           | 0.953       | 0.949          | 0.952       | 0.948          | 0.952       | 0.948          | 0.952       | 0.948          |
| N(1)–C(2)           | 1.465           | 1.453       | 1.451          | 1.439       | 1.438          | 1.398       | 1.393          | 1.398       | 1.393          |
| C(1)–C(7)           | 1.496           | 1.488       | 1.488          | 1.485       | 1.486          | 1.479       | 1.478          | 1.479       | 1.478          |
| C(8)–C(13)          | 1.391           | 1.382       | 1.391          | 1.381       | 1.382          | 1.382       | 1.386          | 1.382       | 1.386          |
| C(11)–C(14)         | 1.508           | 1.511       | 1.510          | 1.510       | 1.510          | 1.509       | 1.509          | 1.509       | 1.509          |
| C(14)–H(14C)        | 0.980           | 1.084       | 1.086          | 1.085       | 1.086          | 1.085       | 1.086          | 1.085       | 1.086          |
| N(1)–H(1C)          | 0.910           | 1.034       | 1.032          | 1.211       | 1.190          | 1.885       | 1.919          | 1.885       | 1.919          |
| O(4)–H(1C)          | 2.176           | 1.846       | 1.830          | 1.262       | 1.282          | 0.976       | 0.968          | 0.976       | 0.968          |
| O(3)–S(1)–O(5)      | 112.98          | 114.2       | 114.2          | 116.7       | 116.7          | 118.9       | 119.8          | 118.9       | 119.8          |
| O(3)–S(1)–C(8)      | 106.19          | 105.3       | 106.7          | 107.6       | 107.5          | 108.9       | 108.5          | 108.9       | 108.5          |
| H(14B)–C(14)–H(14C) | 109.50          | 107.4       | 107.8          | 107.8       | 107.6          | 107.7       | 107.7          | 107.7       | 107.7          |
| O(1)–C(7)–O(2)      | 123.50          | 121.7       | 121.6          | 121.2       | 121.3          | 120.5       | 120.5          | 120.5       | 120.5          |
| O(2)–C(7)–C(1)      | 113.35          | 113.6       | 113.8          | 113.6       | 113.8          | 113.7       | 113.8          | 113.7       | 113.8          |
| C(3)–C(2)–N(1)      | 117.70          | 116.8       | 116.8          | 117.1       | 117.2          | 118.0       | 118.1          | 118.0       | 118.1          |
| C(1)–C(2)–N(1)      | 120.84          | 120.0       | 122.0          | 122.3       | 122.3          | 123.0       | 123.1          | 123.0       | 123.1          |
| H(1B)–N(1)–H(1C)    | 109.50          | 99.36       | 99.4           | 100.6       | 101.0          | 92.3        | 91.7           | 92.3        | 91.7           |
| C(2)–C(1)–C(7)      | 120.94          | 121.6       | 121.7          | 121.5       | 121.5          | 121.1       | 121.1          | 121.1       | 121.1          |
| C(9)–C(8)–C(13)     | 120.21          | 120.0       | 120.0          | 120.3       | 120.3          | 120.8       | 120.8          | 120.8       | 120.8          |
| H(14A)–C(14)–H(14C) | 109.50          | 107.7       | 107.9          | 107.4       | 107.6          | 107.7       | 107.7          | 107.7       | 107.7          |
| C(12)–C(11)–C(14)   | 121.24          | 120.3       | 121.4          | 120.2       | 121.5          | 120.1       | 120.7          | 120.1       | 120.7          |
| C(7)–O(2)–H(2)      | 109.50          | 108.4       | 109.0          | 108.1       | 108.7          | 107.5       | 108.2          | 107.5       | 108.2          |

Bond lengths

Bond angles

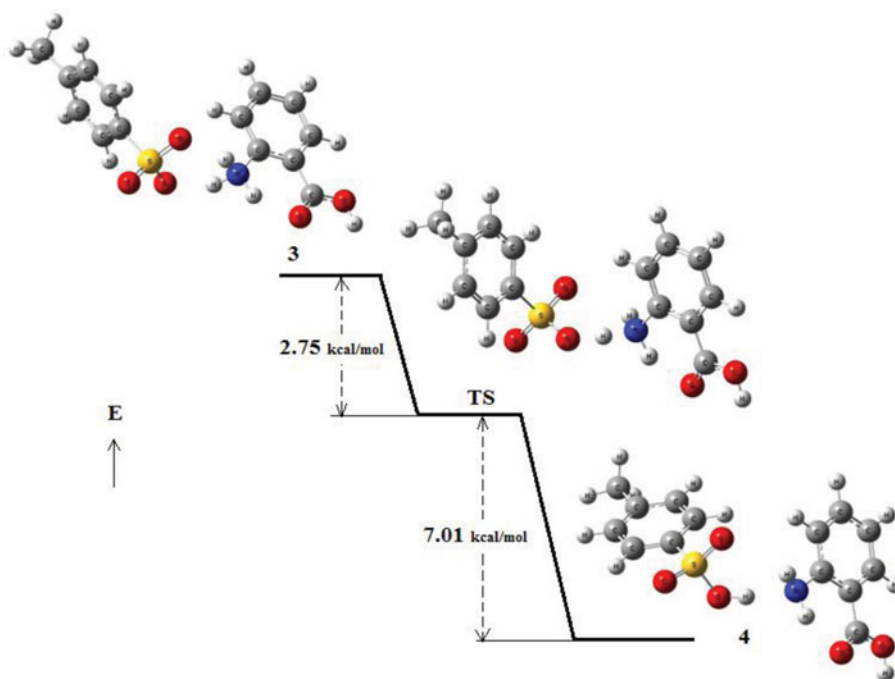


**Figure 3** The optimized geometries and relative energies ( $\Delta E$ , kcal/mol, including the zero-point vibrational energy correction) of ionic form (3), nonionic form (4), and transition state (TS $\rightarrow$ 4) structure at the HF/6-31+G(d,p) level (Color figure available online).

spectrum of this species confirmed by establishing a “one to one” correlation between experiment and theory. In total, there are 102 vibrations from 12 to 4044  $\text{cm}^{-1}$  at the RHF/6-31G(d) level, 5 to 4113  $\text{cm}^{-1}$  at the RHF/6-31+G(d,p) level. As seen from Table S1, the agreement between the experimental and calculated frequencies is reasonably good, especially considering that no scaling is employed.

The hydroxyl vibrations are likely to be the most sensitive to the environment, so they show pronounced shifts in the spectra of the hydrogen-bonded species. The experimental OH-stretching vibrations were observed at around 3500  $\text{cm}^{-1}$ . However, the theoretical values of O-H-stretching modes are found to be larger than the experimental one and this implies that the H atom has an intermolecular hydrogen bonding.<sup>15</sup> Besides, aromatic primary amines display two medium intensity absorption bands: the one near 3500  $\text{cm}^{-1}$  corresponds to the asymmetrical and the other, near 3400  $\text{cm}^{-1}$ , to symmetrical N-H stretching modes.<sup>16</sup> In the ion-pair (3), the bands found at 3478 (calculated at 3681  $\text{cm}^{-1}$ ) and 3195  $\text{cm}^{-1}$  (calculated at 3248  $\text{cm}^{-1}$ ) correspond to the asymmetric and symmetric stretches in the experimental IR spectrum, respectively. The lowering of N-H stretching wavenumbers can be attributed to the intermolecular N-H...O interaction.

The C=O stretching frequencies usually lie in the region between 2000 and 1500  $\text{cm}^{-1}$ . Various other vibrations, such as C=C, C=N stretching and N-H bending vibrations, also occur in this region. However, the C=O stretching is normally more intense than any other vibration in this region. The position of C=O stretching depends upon conjugation, hydrogen bonding, and the size of the ring to which it is attached. In



the IR spectrum of **3**, the  $\nu(\text{C}=\text{O})$  mode was computed at  $1980.9\text{ cm}^{-1}$  and  $1956.0\text{ cm}^{-1}$ , with the HF/6-31G(d) and HF/6-31+G(d,p) theory of level, respectively, and this mode is observed at  $1712\text{ cm}^{-1}$  as a very strong band in the IR spectrum. Due to the association of molecules in the solid phase, the observed C=O stretching frequency is lower than the calculated ones.

### Atomic Charges

The calculation of effective atomic charges plays an important role in the application of quantum chemical calculations to molecular systems.<sup>17,18</sup> Main atomic charges also affect the reactivity of molecules. Atomic charges of the title complex (**3**) have been calculated with help of natural bond orbital (NBO) analysis at HF/6-31G(d) and HF/6-31+G(d,p) levels given in Table S2 (available online). Generally, the theoretical results show that the sulfur atom and oxygen atom (O5) of the sulfite group have the highest positive (+2.690) and negative charge (-1.148) on **3** at the HF/6-31+G(d,p) method, respectively. It is noticed that the carbon atom attached to nitrogen and oxygen atoms (C2 and C7) at both levels is an electron-deficient atom (i.e., it possesses positive charge due to the electronegative character). However, the high negative values are those that are present at nitrogen and oxygen, in the order: N1, O2, and O1. The remaining carbon atoms possess negative electronic charge. The magnitude of the hydrogen atomic charges is found to be only positive and is arranged in an order from 0.222 to 0.520 for the complex **3**. From the calculated results, it will also be possible to say change to charge distribution by a change in the basis sets. The charges depend on the basis set and are changed due to the polarization and diffuse functions used herein.

### Molecular Electrostatic Potential

The molecular electrostatic potential (MEP) is used widely for deciding sites' molecular reactivity, intermolecular interactions, molecular recognition, nucleophilic and electrophilic reactions, as well as hydrogen bonding interactions.<sup>19</sup> To predict reactive sites for electrophilic and nucleophilic attack for the title molecule, MEP was calculated by applying the HF method and the 6-31+G(d,p) basis set for the optimized geometry. The negative (red) regions of MEP were related to the electrophilic reactivity and the positive (blue) regions to nucleophilic reactivity depicted in Figure S1 (available online). As can be seen from the figure, the negative regions of the title structures were observed around the  $\text{SO}_3^-$  part of  $\text{C}_7\text{H}_7\text{O}_3\text{S}^-$ , whereas a maximum positive region is localized on the  $\text{NH}_3^+$  part of  $\text{C}_7\text{H}_3\text{NO}_2^+$  for the complex **3** at the HF/6-31+G(d,p) level. Moreover, there are two possible sites on the title compound for electrophilic attack. The negative regions are mainly over the O3 and O5 atoms. These results provide information concerning the region where the compound can have intra- or intermolecular interaction and metallic bonding. Hence, the MEP map confirms the existence of intra- and intermolecular interactions observed in the solid state.

### Frontier Molecular Orbitals

The frontier molecular orbitals (highest occupied molecular orbital-HOMO and lowest unoccupied molecular orbital-LUMO) are the main orbitals taking part in chemical

reactions.<sup>20</sup> The HOMO energy characterizes the ability of electron donating, LUMO energy characterizes the ability of electron accepting, and the gap between HOMO and LUMO characterizes the molecular chemical stability. It is known that the HOMO–LUMO gap also plays an important role in the electric and optical properties, as well as in UV-Vis spectra and chemical reactions.<sup>21–26</sup> As can be seen from Figure S2 (available online), HOMO of **3** is mainly on  $C_7H_7O_3S^-$  part, whereas LUMO of the structure is substantially localized on  $C_7H_8NO_2^+$  part of title molecule. The values of the energy separation between the HOMO and LUMO for **3**, **4**, and **TS**, also are 0.358, 0.381, and 0.425 eV at HF/6–31+G(d,p) theory of level, respectively. Molecular orbital coefficients analyses based on their optimized geometries indicate that the frontier molecular orbitals are mainly composed of  $\pi$ -atomic orbitals, so the electronic transitions are mainly derived from the contribution of bands  $\pi$ – $\pi^*$ .

### Nucleus-Independent Chemical Shifts (NICS)

Aromaticity (aromatic) is considered as one of the most important concepts in modern organic chemistry.<sup>27</sup> The simplest criterion for aromatic compounds is the presence of cyclic-conjugated  $\pi$ -systems containing the proper number of  $\pi$ -electrons. In 1996, Schleyer proposed a simple and efficient probe for aromaticity: NICS, which is the computed value of the negative magnetic shielding at some selected point in space, generally, at a ring or cage center.<sup>28</sup> The theoretical HF/6–31+G(d) method was applied by Schleyer for the computation of aromaticities for a series of aromatic, antiaromatic, or nonaromatic compounds; it was proposed that negative NICS values indicate aromaticity (–9.7 for benzene), whereas large positive NICS values indicate antiaromaticity (27.6 for cyclobutadiene) and small NICS values denote nonaromaticity (–2.2 for cyclohexane). NICS data for the present systems were computed with the HF/6–31+G(d,p) method at the ring center (NICS(0)). The justification of the applied method was performed by obtaining –9.7, 28.8, and –2.4 for benzene, cyclobutadiene, and cyclohexane, respectively.

The NICS(0) data calculated at the ring center indicate that  $C_7H_7O_3S^-$  and  $C_7H_8NO_2^+$  part of the complex (**3**) have an aromatic character with –10.3 for *Bq1* and –10.9 for *Bq2*, respectively, (see supplemental data, Figure S3, available online), while the NICS values of *p*-toluenesulfonic acid and anthranilic acid are found to be –10.4 for *Bq3* and –8.6 for *Bq4*, respectively (see supplemental data, Figure S4, available online). The NICS value can be affected by other structural features that are not directly related to the aromatic ring current. In fact, the data depict that the NICS value of  $C_7H_7O_3S^-$  part (*Bq1*) of complex (**3**) is almost equal to that of *p*-toluenesulfonic acid, whereas the NICS value of  $C_7H_8NO_2^+$  part (*Bq2*) is by only 2.3 lower than that of anthranilic acid (Table S3, available online).

### CONCLUSION

Success with PTSA is unusual, considering that crystal structures of proton transfer Lewis base compounds with PTSA are uncommon, possibly because of the absence of interactive secondary substituent functional groups to promote hydrogen bonding extension. In this work, PTSA and anthranilic acid form a crystalline complex of stoichiometry 1:1. The X-ray and IR spectral data for the title compound show that one proton from PTSA is transferred to anthranilic acid and the molecules are linked by the N–H...O hydrogen

bonds. The comparisons between the theoretical results and the X-ray single-crystal data indicate that both HF/6–31G(d) and HF/6–31+G(d,p) level are adequate to reproduce the experimental geometric parameters. The vibrational frequencies of **3** are precisely assigned to its molecular structure with the aid of the theoretical calculations at the HF/6–31G(d) and the HF/6–31+G(d,p) levels, in which the experimental and theoretical results support each other. The MEP map shows that the negative potential site is on the  $\text{SO}_3^-$  part of  $\text{C}_7\text{H}_7\text{O}_3\text{S}^-$  while the positive potential sites are around the  $\text{NH}_3^+$  part of  $\text{C}_7\text{H}_8\text{NO}_2^+$  for the complex **3** at the HF/6–31+G(d,p) level. These sites give information about the region from where the compound (**3**) can have intermolecular interactions and metallic bonding.

## EXPERIMENTAL

### General Method

Anthranilic acid (**1**), PTSA (**2**), and solvents were purchased from Sigma–Aldrich Chemical Company (Steinheim, Germany) with a stated purity of greater than 98% and used as such without further purification. Infrared spectrum of 2-carboxyanilinium *p*-toluenesulfonate (**3**) was recorded between 4000 and 400  $\text{cm}^{-1}$  on Perkin-Elmer FTIR spectrophotometer using solid KBr plates. The spectrum was recorded at room temperature, with a scanning speed of 30  $\text{cm}^{-1} \text{min}^{-1}$  and with a spectral resolution of 2.0  $\text{cm}^{-1}$  in the CSL Laboratory, Balikesir University, Turkey.

### Synthesis

The title compound (**3**,  $\text{C}_7\text{H}_8\text{NO}_2^+ \cdot \text{C}_7\text{H}_7\text{O}_3\text{S}^-$ ) was synthesized by the reaction of anthranilic acid (1 mmol) with PTSA (1 mmol) in methanol (50 mL) for 40 min under reflux. After concentration to ca 30 mL of the hot filtered solution, colorless prismatic crystals of (**3**), suitable for X-ray analysis were obtained by slow evaporation at room temperature. m.p. 163–164 °C. Analysis for  $\text{C}_{14}\text{H}_{15}\text{NO}_5\text{S}$  calculated: %C, 54.36; %H, 4.89; %N, 4.53; found: %C, 54.29; %H, 4.92; %N, 4.56.

### Crystal Structure Determination

Diffraction measurements were made on a Bruker ApexII kappa CCD diffractometer using graphite-monochromated  $\text{Mo-K}_\alpha$  radiation ( $\lambda = 0.71073 \text{ \AA}$ ) at 100 K for **3**. The intensity data were integrated using the APEXII program.<sup>29</sup> Absorption corrections were applied based on equivalent reflections using SADABS.<sup>30</sup> The structures were solved by direct methods and refined using full-matrix least squares against  $F^2$  using SHELXL.<sup>17</sup> All nonhydrogen atoms were assigned anisotropic displacement parameters and refined without positional constraints. Hydrogen atoms were included in idealized positions with isotropic displacement parameters constrained to 1.5 times the  $U_{\text{equiv}}$  of their attached carbon atoms for methyl hydrogens, and 1.2 times the  $U_{\text{equiv}}$  of their attached carbon atoms for all others. A possible disorder in the ethanolamine portion of the ligand for the title complex (**3**) has been considered. All of the crystallographic computations were carried out with the help of SHELXTL<sup>31</sup>, MERCURY<sup>32</sup>, and ORTEP-3<sup>33</sup> programs. Details of the data collection parameters and crystallographic information for the complexes are summarized in Table 1.

## COMPUTATIONAL DETAILS

The proton transfer compound (3) and its nonionic form (4) were examined using ab-initio methods implemented in the GAUSSIAN 03W program package.<sup>34,35</sup> Full geometry optimizations without any constraints were performed at the HF/6-31G(d) and the HF/6-31+G(d,p) levels of theory. The vibrational frequencies of the title compound (3) were also calculated at the HF/6-31G(d) and the HF/6-31+G(d,p). Agreement among the two methods is a good indicator that the vibrational modes have been correctly assigned. Each motion (stretching, symmetric stretching, asymmetric stretching, in-plane bending, out-of-plane bending, wagging, scissoring, rocking, twisting, etc.) of normal modes was interpreted by means of visual inspection with the help of the GaussView program.<sup>36</sup> Stationary points were characterized as minima or transition structures by way of an analytic evaluation of harmonic frequencies at the level of geometry optimization. All energy values reported here include unscaled zero-point vibrational energies.

To predict reactive sites for electrophilic and nucleophilic attack for the title molecule, MEP was calculated using the HF/6-31+G(d,p) level. MEP,  $V(\mathbf{r})$ , at a given point  $\mathbf{r}(x,y,z)$  in the vicinity of a molecule, is defined in terms of the interaction energy between the electrical charge generated from the molecule, electrons, and nuclei and positive test charge (a proton) located at  $\mathbf{r}$ . For the systems studied,  $V(\mathbf{r})$  was calculated as described previously, using the equation,<sup>37</sup>

$$V(\mathbf{r}) = \sum_A \frac{Z_A}{|\mathbf{R}_A - \mathbf{r}|} - \int \frac{\rho(\mathbf{r}')}{|\mathbf{r}' - \mathbf{r}|} d\mathbf{r}', \quad (1)$$

where  $Z_A$  is the charge of nucleus  $A$ , located at  $\mathbf{R}_A$ ,  $\rho(\mathbf{r}')$  is the electronic density function of the molecule as obtained from ab-initio calculations, and  $\mathbf{r}'$  is the dummy integration variable.

## Supplemental Data

CCDC 752447 contains the supplementary crystallographic data, Molecular electrostatic potential map, HOMO/LUMO images, nucleus-independent chemical shift (NICS) images, and atomic charges of the structures for this paper. These data can be obtained free of charge via [www.ccdc.cam.ac.uk/retrieving.html](http://www.ccdc.cam.ac.uk/retrieving.html) (or from the Cambridge Crystallographic Data Centre, 12, Union Road, Cambridge, B2 1EZ, UK; fax +44 1223 336033; or [deposit@ccdc.cam.ac.uk](mailto:deposit@ccdc.cam.ac.uk)).

## REFERENCES

1. Wiklund, F.; Bergman, J. *Curr. Org. Synth.* **2006**, *3*, 379-402.
2. Botting, N. P. *Chem. Soc. Rev.* **1995**, *24*, 401-412.
3. Niemann, G. J. *Phytochemistry* **1993**, *34*, 319-328.
4. Aghabozorg, H.; Manteghi, F.; Sheshmani, S. *J. Iran. Chem. Soc.* **2008**, *5*, 184-227.
5. Ilczyszyn, M.; Chwaleba, D.; Ciunik, Z.; Ilczyszyn, M. M. *Chem. Phys.* **2008**, *352*, 57-64.
6. Szafran, Z. D.; Katrusiak, A.; Szafran, M. *J. Mol. Struct.* **2010**, *967*, 80-88.
7. Morales, R. G. E.; Parrini, F.; Vargas, V. *Phosphorus, Sulfur Silicon Relat. Elem.* **1998**, *133*, 1-11.

8. Koşar, B.; Albayrak, Ç.; Ersanlı, C. C.; Odabaşoğlu, M.; Büyükgüngör, O. *Spectrochim. Acta A.* **2012**, *93*, 1-9.
9. Eshtiagh-Hosseini, H.; Aghabozorg, H.; Mirzaei, M.; Beyramabadi, S. A.; Eshghi, H.; Morsali, A.; Shokrollahi, A.; Aghaei, R. *Spectrochim. Acta A.* **2011**, *78*, 1392-1396.
10. Pejov, L.; Ristova, M.; Soptrajanov, B. *Spectrochim. Acta A.* **2011**, *79*, 27-34.
11. Moghimi, A.; Moosavi, S. M.; Kordestani, D.; Maddah, B.; Shamsipur, M.; Aghabozorg, H.; Ramezanipour, F.; Kickelbick, G. *J. Mol. Struct.* **2007**, *828*, 38-45.
12. Ding, X. H.; Cui, L. F.; Li, Y. H.; Wang, S.; Huang, W. *New J. Chem.* **2012**, *36*, 1884-1890.
13. Smith, G.; Wermuth, U. D.; Healy, P. C.; Young, D. J.; White, J. M. *Acta Crystallogr., Sect. E.* **2005**, *61*, o2646-o2648.
14. Smith, G.; Wermuth, U. D.; Healy, P. C.; White, J. M. *Acta Crystallogr., Sect. E.* **2006**, *62*, o5089-o5091.
15. Dal, H.; Süzen, Y.; Şahin, E. *Spectrochim. Acta A.* **2007**, *67*, 808-814.
16. Colthup, N. B.; Daly, L. H.; Wiberley, S. E. *Introduction to Infrared and Raman Spectroscopy*; Academic Press: New York, 1990.
17. Azizoglu, A.; Yildiz, C. B. *Organometallics* **2010**, *29*, 6739-6743.
18. Zinlynezhad, A.; Nori-Shargh, D.; Najma, N.; Yahyaei, H. *Phosphorus, Sulfur Silicon Relat. Elem.* **2011**, *186*, 44-57.
19. Azizoglu, A.; Yildiz, C. B. *J. Organomet. Chem.* **2012**, *715*, 19-25.
20. Fleming, I. *Frontier Orbitals and Organic Chemical Reactions*; Wiley: London, 1976.
21. Sagdinc, S. G.; Kandemirli, F.; Köksoy, B.; Bayari, S. M. *Phosphorus, Sulfur Silicon Relat. Elem.* **2012**, *187*, 1243-1260.
22. Nikolova, R. D. *Phosphorus, Sulfur Silicon Relat. Elem.* **2011**, *186*, 1626-1634.
23. Azizoglu, A.; Ozer, Z.; Kilic, T. *Collect. Czech. Chem. Commun.* **2011**, *76*, 95-114.
24. Septelean, R.; Petrar, P. M.; Nemes, G.; Escudié, J.; Silaghi-Dumitrescu, I. *Phosphorus, Sulfur Silicon Relat. Elem.* **2011**, *186*, 2321-2331.
25. Saracoglu, N.; Talaz, O.; Azizoglu, A.; Watson, W. H.; Balci, M. *J. Org. Chem.* **2005**, *70*, 5403-5408.
26. Azizoglu, A. *Struct. Chem.* **2003**, *14*, 575-580.
27. Krygowski, T. M.; Cyran, M. K.; Czarnocki, Z.; Hafelinger, G.; Katritzky, A. R. *Tetrahedron* **2000**, *56*, 1783-1796.
28. Schleyer, P. v. R.; Maerker, C.; Dransfeld, A.; Jiao, H.; Hommes, N. J. R. E.; *J. Am. Chem. Soc.* **1996**, *118*, 6317-6318.
29. Bruker-AXS SAINT V7.60A.
30. Sheldrick, G. M. *SADABS V2008/1*, University of Göttingen: Germany.
31. Sheldrick, G. M. *SHELXTL Version 5.1*, Program for the Solution and Refinement of Crystal Structures, Bruker AXS, Inc.: Madison, WI, USA, 1999.
32. Mercury version 1.5, *Cambridge Crystallographic Data Centre*; Cambridge, UK, **2006**.
33. Farrugia, L. J. *J. Appl. Crystallogr.* **1997**, *30*, 565-566.
34. Hehre, W. J.; Radom, L.; Schleyer, P. v. R.; Pople, J. A. *Ab-Initio Molecular Orbital Theory*; John Wiley & Sons: New York, 1986.
35. Frisch, M. J.; Trucks, G. W.; Schlegel, H. B.; Scuseria, G. E.; Robb, M. A.; Cheeseman, J. R.; Montgomery, Jr.; J. A.; Vreven, T.; Kudin, K. N.; Burant, J. C.; Millam, J. M.; Iyengar, S. S.; Tomasi, J.; Barone, V.; Mennucci, B.; Cossi, M.; Scalmani, G.; Rega, N.; Petersson, G. A.; Nakatsuji, H.; Hada, M.; Ehara, M.; Toyota, K.; Fukuda, R.; Hasegawa, J.; Ishida, M.; Nakajima, T.; Honda, Y.; Kitao, O.; Nakai, H.; Klene, M.; Li, X.; Knox, J. E.; Hratchian, H. P.; Cross, J. B.; Bakken, V.; Adamo, C.; Jaramillo, J.; Gomperts, R.; Stratmann, R. E.; Yazyev, O.; Austin, A. J.; Cammi, R.; Pomelli, C.; Ochterski, J. W.; Ayala, P. Y.; Morokuma, K.; Voth, G. A.; Salvador, P.; Dannenberg, J. J.; Zakrzewski, V. G.; Dapprich, S.; Daniels, A. D.; Strain, M. C.; Farkas, O.; Malick, D. K.; Rabuck, A. D.; Raghavachari, K.; Foresman, J. B.; Ortiz, J. V.; Cui, Q.; Baboul, A. G.; Clifford, S.; Cioslowski, J.; Stefanov, B. B.; Liu, G.; Liashenko, A.; Piskorz, P.; Komaromi, I.; Martin, R. L.; Fox, D. J.; Keith, T.; Al-Laham, M. A.; Peng, C. Y.; Nanayakkara,

- A.; Challacombe, M.; Gill, P. M. W.; Johnson, B.; Chen, W.; Wong, M. W.; Gonzalez, C.; and Pople, J. A. *Gaussian 03, Revision C.02*, Gaussian, Inc.: Pittsburgh, PA, 2003.
36. Dennington, R. I. I.; Keith, T.; Millam, J.; Eppinnett, K.; Hovell, W. L.; Gilliland, R. *Gaussview, version 3.0*, Gaussian, Inc., Pittsburgh, PA, 2003.
37. Murray, J. S.; Politzer, P. *WIREs Comput. Mol. Sci.* **2011**, 1, 153-163.